Evaluating the anharmonicity contributions to the molecular excited state internal conversion rates with finite temperature TD-DMRG

Yuanheng Wang,[1] Jiajun Ren,[1, a)] and Zhigang Shuai[1, b)]
MOE Key Laboratory of Organic OptoElectronics and Molecular Engineering,
Department of Chemistry, Tsinghua University, Beijing 100084,
People's Republic of China

(Dated: 1 April 2021)

In this work, we propose a new method to calculate the molecular nonradiative electronic relaxation rates based on the numerically exact time-dependent density matrix renormalization group theory (TD-DMRG). This method could go beyond the existing frameworks under the harmonic approximation (HA) of the potential energy surface (PES) so that the important anharmonic effect could be considered when large electronic energy is transferred into the vibrations to excite them to the high energy levels. The effectiveness and scalability of the method are verified in calculating the internal conversion (IC) rate of azulene by comparing it with the analytically exact results under HA. Furthermore, we investigate the validity of HA in a two-mode model with Morse potential. We find that HA is unsatisfactory unless only the lowest several vibrational states of the lower electronic state are involved in the transition process when the adiabatic excitation energy is relatively low. As the excitation energy increases, HA first underestimates and then overestimates the IC rates when the excited state PES shifts towards the dissociative side of the ground state PES. On the contrary, HA slightly overestimates the IC rates when the excited state PES shifts towards the repulsive side. In both cases, higher temperature enlarges the error of HA.

---

a)Electronic mail: renjj@mail.tsinghua.edu.cn
b)Electronic mail: zgshuai@tsinghua.edu.cn

I. INTRODUCTION

Nonradiative electronic relaxation (NRER) is an important process in the photophysics of molecular optoelectronic materials. It includes internal conversion process (IC) between the electronic states of the same spin manifold and intersystem crossing process (ISC) between the electronic states of different spin manifolds.[1] For organic photovoltaics and organic light-emitting system, the NRER processes from the excited state to the ground state is an unfavorable process which dissipates electronic energy into vibrational reservoirs and leads to the reduction of the energy conversion efficiency of the devices. Considering the important role of NRER in the molecular photophysical processes, how to calculate the rate of NRER theoretically has always been a hot topic. [2–9]

Currently, the real-time nonadiabatic dynamics simulation and the rate theory relying on the Fermi's golden rule (FGR) are the two main approaches to study NRER process. Nonadiabatic dynamics directly simulate the nuclear motions over the coupled potential energy surfaces (PES) to obtain the real-time population on each electronic state. Though full-quantum dynamics methods have made great progress in recent years, it is still limited by the system size of complex molecules.[10–12] Even if less accurate, nonadiabatic mixed quantum-classical dynamics (NA-MQC) methods provide a promising way to handle large systems.[13–15] One of the intriguing features of NA-MQC is that it could combine with the modern electronic structure calculation in an on-the-fly fashion to simulate ab-initio dynamics without requiring a precomputed global PES which is necessary in most full-quantum wave-packet methods.[16] Recently, several semiclassical methods have also been extended to simulate the nonadiabatic dynamics combined with the mapping strategy.[17–20] It should be noted that in these methods the anharmonicity of the molecular PES is inherently considered. The main shortcoming of the real-time nonadiabatic dynamics methods to investigate the NRER process is that the accessible timescale is often limited to several picoseconds. Hence, they are suitable to describe the ultrafast transition process, such as transition through the conical intersection where the coupling between the electronic states is very strong.[21] However, the NRER rates of a large portion of useful fluorescent molecules have timescales of nanosecond or even longer,[22] far beyond what the current real-time nonadiabatic dynamics methods could accurately reach.

Complementary to the real-time simulation, in the regime where the coupling between the states is weak, the rate theory based on FGR has been successfully developed to describe the relatively slower processes. The study on this topic has a long history. Robinson and Frosch first outlined the harmonic oscillator approximation model to describe the NRER processes 50 years ago.[23,24] Afterwards, Lin established the framework using the displacement harmonic oscillator model to treat small polyatomic molecules with Duschinsky rotation effect (DRE) (mode-mixing effect) under the promoting mode approximation.[3,25,26] In recent years, Shuai *et al.* have developed an analytical formalism called thermal vibration correlation function (TVCF) to calculate the NRER rate in the time domain.[5,27–29] Under harmonic approximation (HA) of the initial and final electronic PES, this formalism could fully take DRE into consideration and gives the analytically exact transition rates. This method has been successfully used to calculate the NRER rate including IC and ISC processes of a lot of molecules at ab-initio level.[29,30] However, it is known that HA is only valid in the low energy regime around the equilibrium configuration and the higher the energy, the stronger the anharmonic effect, especially for the floppy modes. Consequently, HA may not be reliable to describe the PES of the lower electronic state in the NRER process, because the large electronic excitation energy is dumped into the vibrations resulting in a relatively high vibrational quanta. Some former studies have attempted to investigate the anharmonic effect on the NRER rates of molecules in the FGR framework. Ianconescu and Pollak applied semiclassical initial value representation method to study the IC rate in a two-mode model with Morse potential.[31] They found that HA is mostly unsatisfactory in a wide parameter regime. Humeniuk *et al.* assessed the validity of HA for several coumarin dyes when predicting the fluorescence quantum yields in solution.[32] They found that the accuracy of HA for the radiative decay rate is remarkable, while HA will underestimate the IC rates. Hence, HA will lead to an unreliable prediction of fluorescence quantum yield compared to the experiments. However, their method to deal with the Morse PES is based on the exact diagonalization and sum-of-states approach, which is not scalable to large systems. Though the aforementioned semiclassical method is scalable and seems promising in a model system, further benchmarking is still required to verify the universality. Therefore, it is important to develop a scalable and numerically exact method to calculate NRER rates beyond HA.

In this work, we propose to calculate the NRER rate with the numerically exact time-dependent density matrix renormalization group method (TD-DMRG).[33–36] In recent years, TD-DMRG has emerged as a powerful method to simulate large-scale full-quantum dynamics,[37–44] such as electronic spectroscopy of molecular aggregates, real-time internal conversion in pyrazine, carrier mobility in one-dimensional molecular crystal, *etc*. There are several advantages of TD-DMRG compared to the other numerical methods: (i) The accuracy could be systematically improved by a single parameter; (ii) The Hamiltonian that can be handled is flexible once it could be represented in a sum-of-products form[45,46] and thus TD-DMRG could handle both model anharmonic PES and PES of real molecules after some preprocessing;[47,48] (iii) The scaling of computational cost is polynomial with system size and thus it is scalable for polyatomic molecules; (iv) The time evolution of wavefunction (at zero temperature) and density matrix (at finite temperature) could be simulated in a same framework[49,50]. These advantages make TD-DMRG a suitable method to calculate the molecular NRER rates.

The remaining sections of this paper are arranged as follows: In section II. THEORY, the Hamiltonian and method are described. In section III. RESULTS & DISCUSSIONS, firstly the IC rate of azulene under HA is calculated and compared with the analytically exact results to demonstrate the effectiveness and scalability of the method. Secondly, IC rate of a two-mode model system with Morse potential are investigated to assess the validation of HA at different circumstances. Unlike the harmonic potential, the IC rate with the Morse potential is not analytically solvable. Finally, the conclusion is presented in section IV. CONCLUSION.

II. THEORY

A. Hamiltonian and transition rate

The molecular Hamiltonian of two uncoupled electronic states could be expressed as Eq. (1), where the mass-weighted coordinates are used. The potential energy operator is expanded by the two adiabatic electronic states $|\psi_i\rangle$, $|\psi_f\rangle$.

$$\hat{H}_0 = \sum_{l=1}^{N} \frac{\hat{p}_l^2}{2} + \begin{bmatrix} U_f + V_f(q_1, q_2, \cdots, q_N) & 0 \\ 0 & U_i + V_i(q_1, q_2, \cdots, q_N) \end{bmatrix} \tag{1}$$

$U_{i/f}$ is the minimal energy of PES at equilibrium configuration. To set up the Hamiltonian for a specific molecule, the difficulty is how to obtain the (semi-)global PES $V_{i/f}$. Even nowadays, it is still a hard task to obtain a (semi-)global PES for polyatomic molecules with more than 20 atoms. The cut-high dimensional model representation (cut-HDMR) or called n-mode representation method[51,52] and the high-order Taylor expansion method[53,54] are two practical methods to include the anharmonicity for large systems. Under HA, this difficulty is bypassed and only two normal mode analysis at the equilibrium configuration are required. The PES can be simplified with the normal coordinates.

$$V_{i/f} = \sum_l \frac{1}{2}\omega_{i/f,l}^2 q_{i/f,l}^2 \tag{2}$$

The normal coordinates of the initial and final states are connected by the Duschinsky rotation matrix S and the normal-mode projected displacement Δq as Eq. (3). The method to calculate these two parameters at ab-initio level has been well established.[28,55,56]

$$q_{f,m} = \sum_l S_{ml} q_{i,l} - \Delta q_{f,m} \tag{3}$$

The perturbation operator that couples the two electronic states is denoted as $\hat{H}_1$. In the IC process, $\hat{H}_1$ is the first order nonadiabatic coupling operator as Eq. (4).

$$\hat{H}_1 = \sum_m \left(\langle \psi_i | \hat{p}_m | \psi_f \rangle | \psi_i \rangle \langle \psi_f | + \text{h.c.} \right) \hat{p}_m \tag{4}$$

In the ISC process, $\hat{H}_1$ is the spin-orbit coupling operator.

$$\hat{H}_1 = \langle \psi_i | \hat{V}_{\text{SOC}} | \psi_f \rangle | \psi_i \rangle \langle \psi_f | + \text{h.c.} \tag{5}$$

When the coupling is weak, it is appropriate to calculate the transition rate between the two electronic states with FGR:

$$W_T = \frac{2\pi}{\hbar} \sum_{i,f} P_i |H_{1,if}|^2 \delta(E_f - E_i) \tag{6}$$

P_i is the Boltzmann distribution of the initial state i at temperature T. We calculate W_T in the time domain by Fourier transform of the Dirac function, the Eq. (7). Hence, the key to calculate the rate is to calculate the time correlation function (TCF) shown in Eq. (9).

$$\delta(E_f - E_i) = \frac{1}{2\pi\hbar} \int_{-\infty}^{\infty} e^{-i(E_f - E_i)t/\hbar}\, dt \tag{7}$$

$$W_T = \frac{1}{\hbar^2} \int_{-\infty}^{\infty} \langle \hat{H}_1(t) \hat{H}_1 \rangle_T \, dt \tag{8}$$

$$\langle \hat{H}_1(t) \hat{H}_1 \rangle_T = \text{Tr}\Big(\frac{1}{Z} e^{-\beta \hat{H}_0} e^{i\hat{H}_0 t/\hbar} \hat{H}_1 e^{-i\hat{H}_0 t/\hbar} \hat{H}_1\Big) \tag{9}$$

At $T = 0$, TCF could be further simplified to Eq. (10),

$$\langle \hat{H}_1(t) \hat{H}_1 \rangle = e^{iE_0 t/\hbar} \langle 0 | \hat{H}_1 e^{-i\hat{H}_0 t/\hbar} \hat{H}_1 | 0 \rangle \tag{10}$$

where $|0\rangle$ is lowest eigenstate of the initial PES. In this work, we focus on the rate of IC process with nonadiabatic coupling operator as Eq. (4). But the rate of ISC process could be calculated in the same manner. For IC with the Condon approximation,

$$|H_{1,if}|^2 = |\langle\phi_i|\langle\psi_i|\hat{H}_1|\psi_f\rangle|\phi_f\rangle|^2 = \sum_{m,n} I_m^* I_n \tag{11}$$

$$I_m = \langle\psi_i|\hat{p}_m|\psi_f\rangle\langle\phi_i|\hat{p}_m|\phi_f\rangle \tag{12}$$

where $\phi_{i/f}$ is the vibrational wavefunction. From Eq. (11), we can find that $|H_{1,if}|^2$ is a summation over two parts: diagonal terms with $n = m$ and off-diagonal terms with $n \neq m$. If the vibrational degrees of freedom (DoF) are uncoupled, I_m could be further simplified as

$$I_m = \langle\psi_i|\hat{p}_m|\psi_f\rangle\langle\chi_i(q_m)|\hat{p}_m|\chi_f(q_m)\rangle \prod_{l\neq m}\langle\chi_i(q_l)|\chi_f(q_l)\rangle, \tag{13}$$

where $\chi(q_m)$ is the eigenstate of a single DoF q_m.

B. TD-DMRG method

In TD-DMRG, the wavefunction ansatz is

$$|\Psi\rangle = \sum_{\{a\},\{\sigma\}} C_{\sigma_1\sigma_2\ldots\sigma_N}|\sigma_1\sigma_2\ldots\sigma_N\rangle \tag{14}$$

$$= \sum_{\{a\},\{\sigma\}} A_{a_1}^{\sigma_1}A_{a_1,a_2}^{\sigma_2}\ldots A_{a_{N-1}}^{\sigma_N}|\sigma_1\sigma_2\ldots\sigma_N\rangle \tag{15}$$

where $|\sigma_i\rangle$ is the orthonormal primitive basis set for each DoF. N is the total number of DoFs in the system. As the full-rank coefficient $C_{\sigma_1\sigma_2\ldots\sigma_N}$ is approximated as the product of a chain of rank-3 matrix $A_{a_{i-1},a_i}^{\sigma_i}$, this ansatz is called a matrix product state (MPS).[50] The dimension of a_i is called the (virtual) bond dimension, denoted as M_S. It is worth noting that the accuracy of an MPS could be systematically improved with M_S. The dimension of σ_i is called the physical bond dimension, denoted as d. In this work, we use the simple harmonic oscillator basis to expand each DoF. If necessary, the discrete variable representation (DVR)[57] is used to approximate the matrix elements of potential energy operator such as the Morse-type operator. Similar to the wavefunction, a common operator $\hat{O}$ can also be represented in the matrix product form, called matrix product operator (MPO), as shown in Eq. (16).

$$\hat{O} = \sum_{\{w\},\{\sigma\},\{\sigma'\}} W_{w_1}^{\sigma_1'\sigma_1}W_{w_1,w_2}^{\sigma_2'\sigma_2}\ldots W_{w_{N-1}}^{\sigma_N'\sigma_N}|\sigma_1'\sigma_2'\ldots\sigma_N'\rangle\langle\sigma_N\sigma_{N-1}\ldots\sigma_1| \tag{16}$$

With MPO, it is convenient to represent $\hat{O}|\Psi\rangle$ as another enlarged MPS with bond dimension $M_O M_S$.

$$\hat{O}|\Psi\rangle = \sum_{\{w,a\},\{\sigma'\}} A'^{\sigma_1'}_{\{w,a\}_1} A'^{\sigma_2'}_{\{w,a\}_1,\{w,a\}_2} \ldots A'^{\sigma_N'}_{\{w,a\}_{N-1}} |\sigma_1'\sigma_2'\ldots\sigma_N'\rangle \tag{17}$$

where

$$A'^{\sigma_i'}_{\{w,a\}_{i-1},\{w,a\}_i} = \sum_{\sigma_i} W^{\sigma_i'\sigma_i}_{w_{i-1},w_i} A^{\sigma_i}_{a_{i-1},a_i} \tag{18}$$

In Eq. (10), the initial state $|0\rangle$ at zero temperature can be obtained through the typical DMRG ground state algorithms by iteratively optimizing each local matrix A.[34,50] At finite temperature, to obtain the thermal equilibrium density matrix $\rho_\beta = \frac{e^{-\beta \hat{H}_0}}{Z(\beta)}$ for a canonical ensemble, the imaginary-time Schrödinger equation is integrated from $\tau = 0$ to $\tau = \beta/2$.

$$-\frac{\partial}{\partial \tau}\rho(\tau) = \hat{H}_0 \rho(\tau) \tag{19}$$

The initial state $\rho(0)$ at infinitely high temperature ($\beta = 0$) is a locally maximally entangled state, which is easily represented as an MPO with $M_O = 1$.

$$\rho(0) = \prod_i \sum_{\sigma_i} \frac{1}{\sqrt{d}} |\sigma_i\rangle\langle\sigma_i| \tag{20}$$

$\rho(\tau)$ is normalized with condition $\langle\langle\rho(\tau)|\rho(\tau)\rangle\rangle = \mathrm{Tr}(\rho(\tau)^\dagger \rho(\tau)) = 1$ after each step of time-evolution. Therefore, $\rho(\beta/2) = e^{-\beta \hat{H}_0/2}/\sqrt{Z(\beta)} = \rho_\beta^{1/2}$. Hence, the TCF in Eq. (9) can be re-expressed as:

$$C(t) = \mathrm{Tr}\big(\rho_\beta^{1/2} e^{i\hat{H}_0 t/\hbar} \hat{H}_1 e^{-i\hat{H}_0 t/\hbar} \hat{H}_1 \rho_\beta^{1/2}\big) \tag{21}$$

This method could equivalently be formulated according to the thermal field dynamics method, also known as the purification method by introducing an auxiliary space.[49,50]

There are many time evolution schemes to propagate the wavefunction and density matrix according to the Schrödinger equation along the real-time or imaginary-time axes, and they are thoroughly compared in Ref. 58 and Ref. 59. In this work, we adopt the time-dependent variational principle based evolution schemes. The variable-mean-field (VMF) scheme is used to propagate the wavefunction with matrix unfolding[60] and adaptive Dormand-Prince's 5/4 Runge-Kutta algorithm. The second order projector-splitting scheme (PS) is used to propagate the density matrix for higher efficiency. Readers are referred to our former works for more details about the derivation and implementation.[59] The computational cost of a single time-step is $O\big(N(M_S^2 M_O^2 d^2 + M_S^3 M_O d + M_S^3 d^2)\big)$ for the former and $O\big(N(M_S^2 M_O^2 d^4 + M_S^3 M_O d^2)\big)$ for the latter, which are both polynomial with system size. All the calculations in the next section are carried out with our in-house code Renormalizer.[61]

III. RESULTS & DISCUSSIONS

A. IC rate of azulene under HA

To verify the correctness of the implementation and demonstrate the effectiveness and scalability of the method, in this section we calculate the rate k_{ic} of IC process of azulene from the S_1 state to S_0 state under HA. This molecule has often been used as a prototypical system to benchmark new methods.[7,28] Under HA, the TVCF method[5,27] (implemented in MOMAP[62]) is analytically exact and thus serves as a reference. The equilibrium configuration and normal mode analysis of the ground state and excited state of azulene are calculated by density functional theory (DFT) and time-dependent DFT at B3LYP/6-31G(d) level in Gaussian 16.[63] The number of normal modes of azulene is 48. The Duschinsky rotation matrix S and normal mode projected displacement Δq as in Eq. (3) are calculated by MOMAP.[62] In the TD-DMRG calculations, the coordinates used are the normal coordinates of the ground state. The time step is 0.25 fs and the total time of simulation is 425 fs. The primitive basis for each DoF is the harmonic oscillator basis up to 20 quanta. The TCF $C(t)$ in Eq. (21) calculated by TVCF and TD-DMRG with different bond dimension M_S are shown in Fig. 1. The results with $M_S = 2$ (blue dashed line) deviate from the exact value after 40 fs and thus is not accurate enough to calculate k_{ic} (See Table.I). The results with $M_S = 20$ (red dashed line) are consistent with the exact values at the resolution scale shown in Fig. 1. The tran-

TABLE I. The internal conversion rate k_{ic} of azulene from the S_1 state to the S_0 state with harmonic approximation calculated by the analytically exact TVCF method and TD-DMRG method with different bond dimension M_S.

Method		$k_{\mathrm{ic}}(\times 10^{10}\,\mathrm{s}^{-1})$ at 0 K	$k_{\mathrm{ic}}(\times 10^{10}\,\mathrm{s}^{-1})$ at 300 K
TVCF		2.14	2.41
TD-DMRG	$M_S = 2$	0.44	1.31
	$M_S = 5$	1.30	1.85
	$M_S = 10$	1.98	2.21
	$M_S = 20$	2.11	2.32
	$M_S = 40$	2.15	2.40
	$M_S = 60$	2.16	2.41

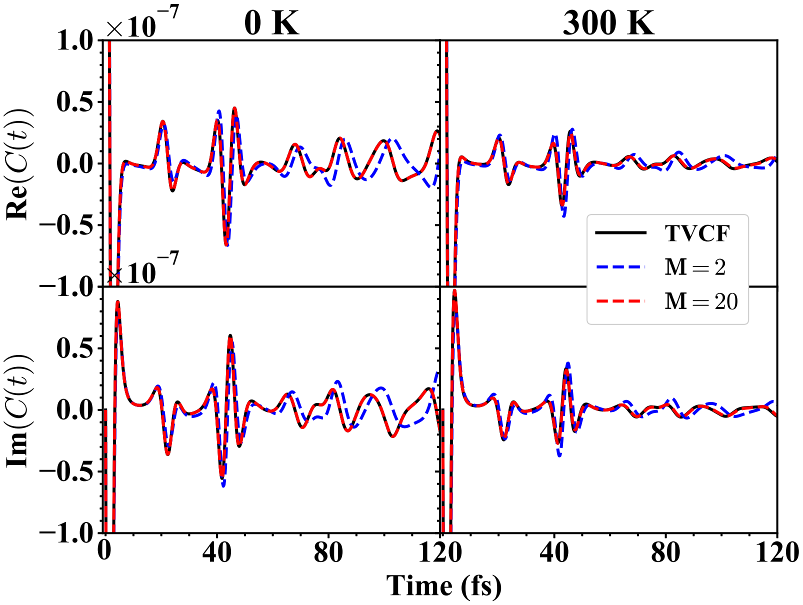

FIG. 1. The real and imaginary part of the time correlation function $C(t)$ at $T = 0\,\mathrm{K}$ and $T = 300\,\mathrm{K}$ calculated by the analytically exact TVCF method implemented in MOMAP[62] (black solid line) and TD-DMRG with bond dimension $M_S = 2$ (blue dashed line) and $M_S = 20$ (red dashed line).

sition rates k_{ic} are listed in Table. I. A Lorentzian broadening factor $100\,\mathrm{cm}^{-1}$ is applied to make the time-integration of TCF converge. The analytically exact value is $2.14 \times 10^{10}\,\mathrm{s}^{-1}$ at $0\,\mathrm{K}$ and $2.41 \times 10^{10}\,\mathrm{s}^{-1}$ at $298\,\mathrm{K}$. The results of TD-DMRG converge very fast with M_S and $M_S = 20$ could obtain a quantitatively accurate rate —— $2.11 \times 10^{10}\,\mathrm{s}^{-1}$ at $0\,\mathrm{K}$ and $2.32 \times 10^{10}\,\mathrm{s}^{-1}$ at $298\,\mathrm{K}$. The computational wall-clock time for the whole simulation with $M_S = 20$ is 51 minutes at $0\,\mathrm{K}$ and 12 hours 17 minutes at $300\,\mathrm{K}$. Though it is much more expensive than the TVCF method under HA, the proposed method based on TD-DMRG could go beyond HA and the cost is not expected to increase too much depending on the specific form of the anharmonic PES.

B. Two-mode model with Morse potential

Although TD-DMRG is not limited to the small systems, in this section we adopt a minimal two-mode model with Morse potential as Ref. 31 to investigate the anharmonic effect on the internal conversion rate from the excited state to the ground state, in which PES of the ground state is characterized by two independent Morse potential along each vibrational DoF, while PES of the excited state is still harmonic (Typically, the excited state is prepared at low energies where a harmonic approximation is reasonable). Even though this model seems simple, unlike the harmonic potential, the internal conversion rate with the Morse potential cannot be calculated analytically. The form of PES could be regarded as the 1-mode representation of a more complex PES.[52] In addition, there is no mode-mixing between the two PESs in the current model. The potential operator is

$$V_i = V_\mathrm{e} = \sum_{l=1,2} \frac{1}{2}\omega_{\mathrm{e},l}^2 q_{\mathrm{e},l}^2 \tag{22}$$

$$V_f = V_\mathrm{g} = \sum_{l=1,2} D_l (1 - e^{-\alpha_l q_{\mathrm{g},l}})^2 \tag{23}$$

$$q_{\mathrm{e},l} = q_{\mathrm{g},l} - \Delta q_l \tag{24}$$

$$U_i - U_f = E_\mathrm{ad} \tag{25}$$

where E_ad is the adiabatic excitation energy. The two parameters to define a Morse potential is the dissociation energy D and the 'width' of the potential well $1/\alpha$. A schematic diagram of the potential energy curve along one coordinate is shown in Fig. 2. A positive/negative Δq represents that the excited state PES is shifted towards the dissociative/repulsive side of the ground state PES.

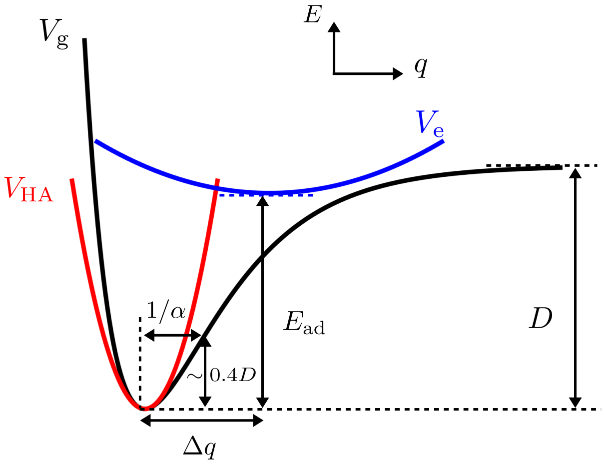

FIG. 2. A schematic diagram of the potential energy curve of the two-mode model along one coordinate. The black curve is the Morse potential $V_g = D(1 - e^{-\alpha q})^2$ of the ground state. The red curve is the harmonic approximation of the Morse potential at the equilibrium position. The blue curve is the harmonic potential of the excited state.

In order to compare with the results in Ref. 31, the same parameters are adopted here, $D_1 = D_2 = D = 5.52\,\mathrm{eV}$ and $\alpha_1 = \alpha_2 = \alpha = 2.23\,\mathrm{amu}^{-1/2}\mathrm{\mathring{A}}^{-1}$ (0.0277 a.u.). Under HA, the harmonic frequency at the equilibrium position is $\omega_{\mathrm{g},1} = \omega_{\mathrm{g},2} = \omega_{\mathrm{g}} = \sqrt{2\alpha^2 D} = 3868\,\mathrm{cm}^{-1}$. The harmonic excited state PES has $\omega_{\mathrm{e},1} = \omega_{\mathrm{e},2} = \omega_{\mathrm{e}} = 774\,\mathrm{cm}^{-1}$. In addition, the displacements are the same for the two DoFs $\Delta q_1 = \Delta q_2 = \Delta q$. The derivative coupling along each coordinate is set to be the same $\langle \psi_{\mathrm{e}} | \frac{\partial}{\partial q_1} | \psi_{\mathrm{g}} \rangle = \langle \psi_{\mathrm{e}} | \frac{\partial}{\partial q_2} | \psi_{\mathrm{g}} \rangle = C$. Hence, the generalized internal conversion rate is defined as $k_{\mathrm{ic}} = W_T / C^2$ using the constant C^2 as the unit. As in Ref. 31, TCF is multiplied by a Gaussian type broadening factor to make it converge after a finite period of time.

$$W_T = \frac{1}{\hbar^2} \int_{-\infty}^{\infty} \langle \hat{H}_1(t) \hat{H}_1 \rangle_T \, e^{-\frac{\sigma(E_{\mathrm{e}})^2 t^2}{2\hbar^2}} \, dt \tag{26}$$

$\sigma(E_{\mathrm{e}})$ is chosen to represent the mean energy interval between the successive vibrational states on the ground state.

$$N(E_{\mathrm{e}}) = \mathrm{Tr}[\Theta(E_{\mathrm{e}} - \hat{H}_{\mathrm{g}})] \approx \frac{1}{2}[(\frac{E_{\mathrm{e}}}{\hbar\omega_{\mathrm{g}}})^2 + \frac{E_{\mathrm{e}}}{\hbar\omega_{\mathrm{g}}}] \tag{27}$$

$$\sigma(E_{\mathrm{e}}) = \frac{\mathrm{d}E_{\mathrm{e}}}{\mathrm{d}N} \tag{28}$$

where Θ is the Heaviside step function and $N(E_{\mathrm{e}})$ is the number of quantum states below E_{e}. E_{e} is the lowest energy of the excited vibronic state. As Ref. 31, the actual $\sigma(E_{\mathrm{e}})$ used in all the calculations is 7 times the value defined in Eq. (27),(28). Since in the current model the two modes are not coupled or mixed, the formal propagator $e^{\hat{H}_{\mathrm{g/e}}\tau}$ could be exactly represented as an MPO with $M_O = 1$, and the initial state $|0\rangle$ at zero temperature or $\rho(0)$ at finite temperature is also a Hartree product state with $M_S = 1$. In addition, $\hat{H}_1$ could be represented as an MPO with $M_O = 2$. Therefore, during the time-evolution, the time-dependent wavefunction in Eq. (10) and Eq. (21) could be exactly represented as an MPS with at least $M_S = 2$ (The numerical results with different M_S are shown in Fig. S1 in the supplementary material.). It should be mentioned that in Ref. 31, the Hamiltonian includes a momentum coupling term $\hat{p}_1 \hat{p}_2 / M$. Since this term is found to have only a minor effect on k_{ic}, it is neglected in the current work. In the subsequent numerical results, the time step is 8 a.u. (about 0.2 fs). The total simulation time is 240 a.u. to obtain the TCF using TD-DMRG and then k_{ic} is calculated according to Eq. (26). We note that in Ref. 31, only the diagonal terms $n = m$ of the summation in Eq. (11) are included to calculate k_{ic} and the off-diagonal terms $n \neq m$ are all neglected. This approximation is similar to the widely known promoting mode approximation,[3] which is valid in the case that only one mode called promoting mode has an appreciable derivative coupling and its displacement is approximately zero. However, considering that this approximation may not always be suitable for all systems, we include the off-diagonal terms when calculating the internal conversion rates.

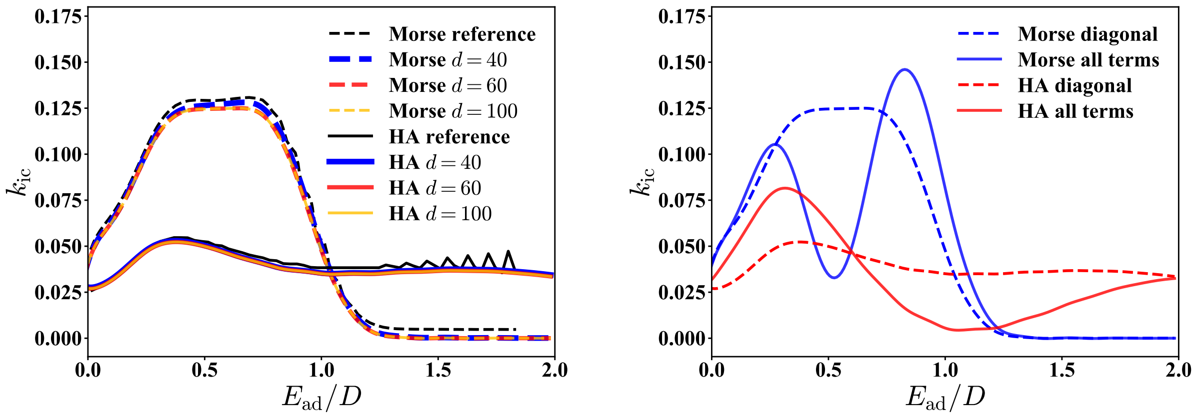

(a) (b)

FIG. 3. a) The dependence of k_{ic} on the adiabatic excitation energy E_{ad}/D at zero temperature calculated by TD-DMRG with different size of primitive basis set. Only the diagonal terms in Eq. (11) are included. The results in Ref. 31 are also plotted for comparison (black line). b) k_{ic} with or without the off-diagonal terms in Eq. (11) calculated by TD-DMRG with $d = 60$. (The displacement is $\Delta q = 0.7/\alpha$. The virtual bond dimension used are $M_S = 4$. Morse: full treatment of the anharmonic Morse PES. HA: harmonic approximation of the Morse potential.)

First, we consider the zero temperature case in which the initial state is the lowest vibronic state of the excited state with zero vibrational quanta in each normal coordinate. With $\Delta q = 0.7/\alpha$ fixed, k_{ic} with different E_{ad} is shown in Fig. 3a in which only the diagonal terms in Eq. (11) are included. The results of TD-DMRG have already converged with physical bond dimension $d = 60$ (the largest quanta of the harmonic oscillator basis) and are consistent with the results of Ref. 31 by the semi-classical initial value representation approach. However, Fig. 3b shows that the off-diagonal terms are also very important in this model, which increase k_{ic} in some regimes and decrease it in the other regimes according to the different E_{ad}. This difference can be attributed to that the off-diagonal terms have different signs when the final vibronic state varies. Fig. 4 shows the relative size of the matrix elements of the off-diagonal terms to that of the diagonal terms $2I_1I_2/(|I_1|^2+|I_2|^2)$, whose value is between -1 and 1.

Since the Morse potential is asymmetrical unlike the harmonic potential, the direction of the relative displacement Δq between the two PESs matters. Fig. 5 shows the 2D contour of the ratio of $k_{\mathrm{ic}}^{\mathrm{Morse}}$ on the Morse potential to $k_{\mathrm{ic}}^{\mathrm{HA}}$ on the harmonic potential with different displacement Δq and adiabatic excitation energy E_{ad} at temperature $T = \omega_{\mathrm{g}}/5$. At three representative displace-

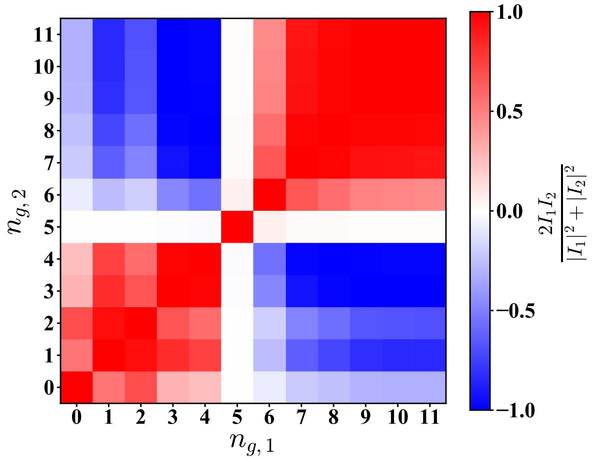

FIG. 4. The relative size of the matrix elements of the off-diagonal terms to that of the diagonal terms $2I_1I_2/(|I_1|^2+|I_2|^2)$ defined in Eq. (11) and Eq. (12) at zero temperature. The vibrational wavefunction $\phi_{\mathrm{g}}(q_1,q_2)=\chi^{\mathrm{HA}}_{n_{\mathrm{g},1}}(q_1)\chi^{\mathrm{HA}}_{n_{\mathrm{g},2}}(q_2)$ of the final state is characterized by two quantum number——$n_{\mathrm{g},1}$ and $n_{\mathrm{g},2}$, which are both ranging from 0 to 11.

ments $\Delta q=0.7/\alpha$, $0/\alpha$ and $-0.52/\alpha$, k_{ic} with different temperatures are shown in Fig. 5b, 5c and 5d. The convergence of the primitive basis set is shown in Fig. S2, S3 and S4 of the supplementary material. It is obvious that HA could give accurate results when E_{ad} is relatively small ($E_{\mathrm{ad}}/D\sim 0$). In this regime, only the vibronic state at the bottom of the ground state PES is involved in the transition process. For this low-energy state, HA is valid as expected. This situation would be encountered in the charge/energy transfer process between molecules of the same kind and ISC process in which the energies of the singlet and triplet state are very close such as the thermally activated delayed fluorescence system.[64] However, a higher energy and a larger positive displacement make the HA-valid regime much narrower. In the regimes that HA obviously fails, two trends can be found within the current model:

1. When the excited state PES shifts towards the dissociative side of the ground state PES ($\alpha\Delta q>0$, the top half of Fig. 5a), HA will first underestimate k_{ic} and then overestimate k_{ic} as E_{ad} increases. In addition, k_{ic} with the Morse potential drops much rapidly as E_{ad} increases compared to that with harmonic potential once the peak is passed (Fig. 5b, 5c).

2. When the excited state PES shifts towards the repulsive side of the ground state PES ($\alpha\Delta q<0$, the bottom half of the Fig. 5a), HA slightly overestimates k_{ic} (Fig. 5d).

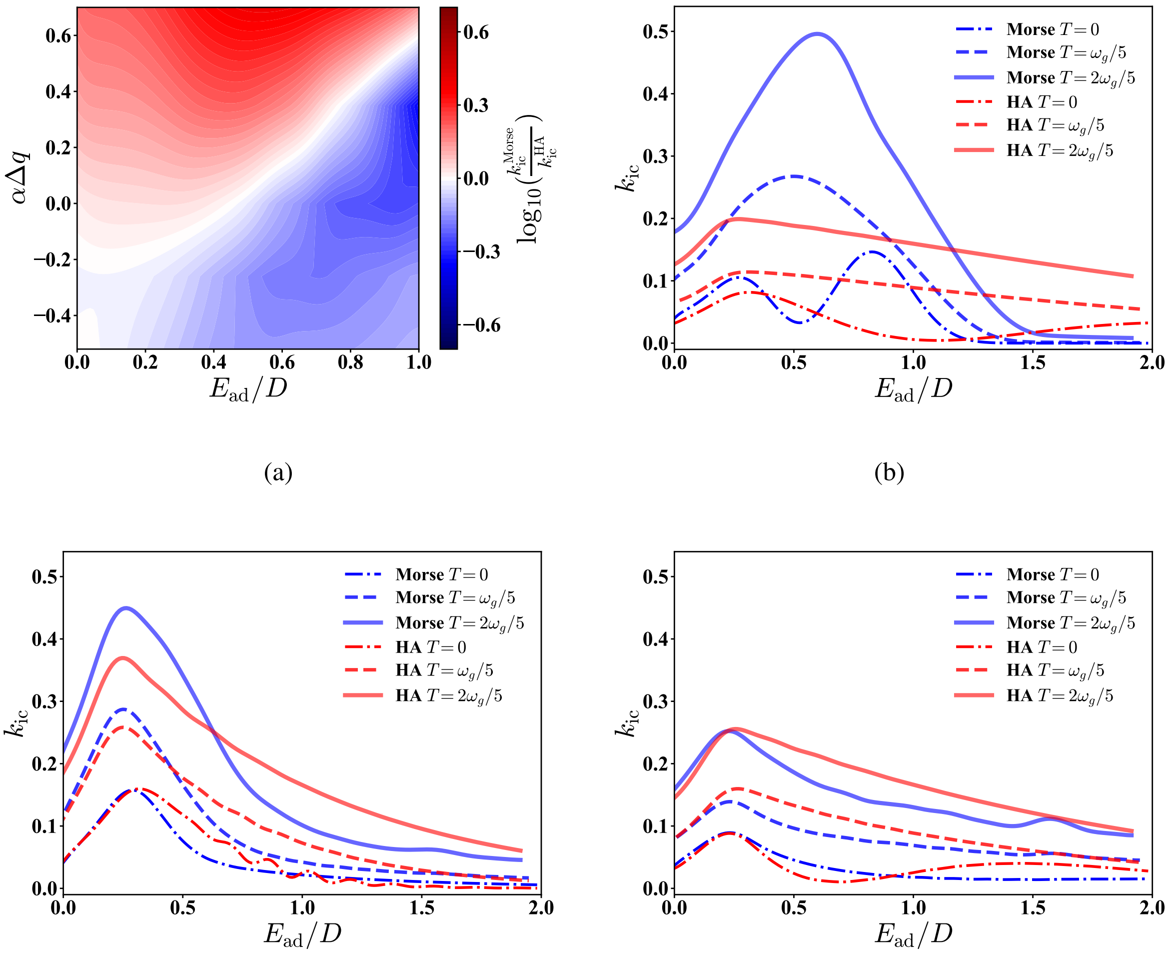

(a)

(b)

(c)

(d)

FIG. 5. a) The ratio of the internal conversion rate on the Morse potential with respect to that under HA with different displacements and adiabatic excitation energies. The temperature is $T = \omega_{\rm g}/5$. b)-d) The dependence of $k_{\rm ic}$ on the adiabatic excitation energy calculated by TD-DMRG with different displacements b) $\Delta q = 0.7/\alpha$, c) $\Delta q = 0/\alpha$ and d) $\Delta q = -0.52/\alpha$, at different temperatures ($T = 0$, $\omega_{\rm g}/5$, $2\omega_{\rm g}/5$), with or without HA. The physical and virtual bond dimension in all these calculations are $d = 100$ and $M_S = 4$. The comparison of the results with different d is shown in the supplementary material.

To examine the generality of the trends described above, we also calculate $k_{\rm ic}$ with $D' = D$, $\alpha' = 2/3\alpha$ and $D' = 4/9D$, $\alpha' = \alpha$. The similar 2D contours as Fig. 5a are shown in Fig. S5 of the supplementary material. The trends are qualitatively the same. Besides these two trends, in both cases, the higher the temperature, the greater the error of HA.

Two fundamental differences between the vibrational wavefunctions of Morse potential $\chi^{\rm Morse}$

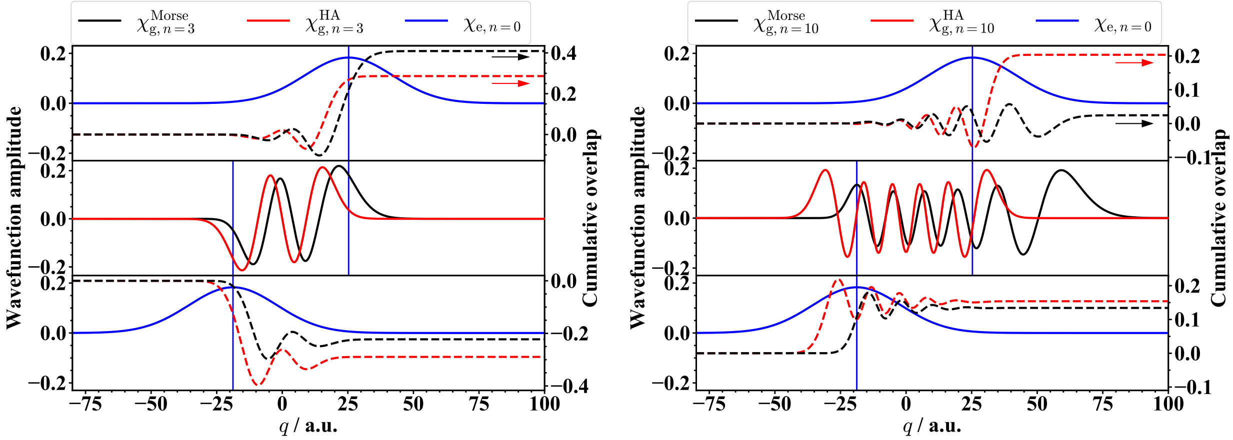

(a)

(b)

FIG. 6. a) Middle panel: the vibrational wavefunction of the ground state with quantum number $n = 3$ on the Morse potential (solid black) and approximated harmonic potential under HA (solid red). Upper panel: the lowest vibrational wavefunction of the excited state with $\Delta q = 0.7/\alpha$ (solid blue) and the cumulative overlap between the initial and final wavefunctions (dashed black and red lines). Lower panel: same as the upper panel but with $\Delta q = -0.52/\alpha$. b) same as (a) but the quantum number of vibrational state of the electronic ground state is $n = 10$.

and harmonic potential χ^{HA} with the same quantum number n may explain the two trends. First, the amplitude of χ^{Morse} is larger than χ^{HA} on the dissociative side, while smaller on the repulsive side, as shown in the middle panels of Fig. 6a ($n = 3$) and Fig. 6b ($n = 10$). Second, by comparing these two panels, χ^{Morse} spreads very fast to the dissociative side as the quantum number increases, while χ^{HA} with the same quantum number is relatively localized. Consequently, when $\alpha\Delta q > 0$ and the quantum number of the final vibrational state is small (E_{ad} is small), the larger amplitude of χ^{Morse} in the region of the initial vibrational wavefunction $\chi_{\text{e}}(n = 0)$ will result in a larger overlap $S^{\text{Morse}}_{\text{g,e}}$ and thus a larger Franck-Condon (FC) factor as shown in the the upper panel of Fig. 6a ($n = 3$) and so is the transition rate k_{ic}. As the quantum number increases, χ^{Morse} quickly spreads to the dissociative side and the amplitude of χ^{Morse} in the region of χ_{e} decays much more rapidly once the large head of χ^{Morse} crosses χ_{e} compared to the more localized χ^{HA}, resulting in a smaller FC factor as shown in the upper panel of Fig. 6b ($n = 10$). Quantitatively, $S^{\text{Morse}}_{\text{g,e}}$ decreases from 0.4 to 0.025 while $S^{\text{HA}}_{\text{g,e}}$ only decreases from 0.3 to 0.2 when the quantum number increases from 3 to 10. In addition, χ^{Morse} has more nodes than χ^{HA} with similar excitation energy, leading to a more serious phase cancellation when calculating the overlap. On the repulsive side, though

χ^{Morse} is also localized, the amplitude of χ^{Morse} is smaller than that of χ^{HA}, resulting in a smaller overlap as shown in the lower panel of Fig. 6a and Fig. 6b. To understand the temperature effect, Fig. 7 shows that the square of matrix element $\langle\chi_{\mathrm{e}}(q)|\frac{\partial}{\partial q}|\chi_{\mathrm{g}}(q)\rangle$ in Eq. (13) (playing the role as a prefactor of the FC factor) is relatively larger for initial state with higher vibrational quanta n_{e}. Therefore, when the thermally populated initial states with higher vibrational quanta get involved with the temperature, the error of HA is significantly larger.

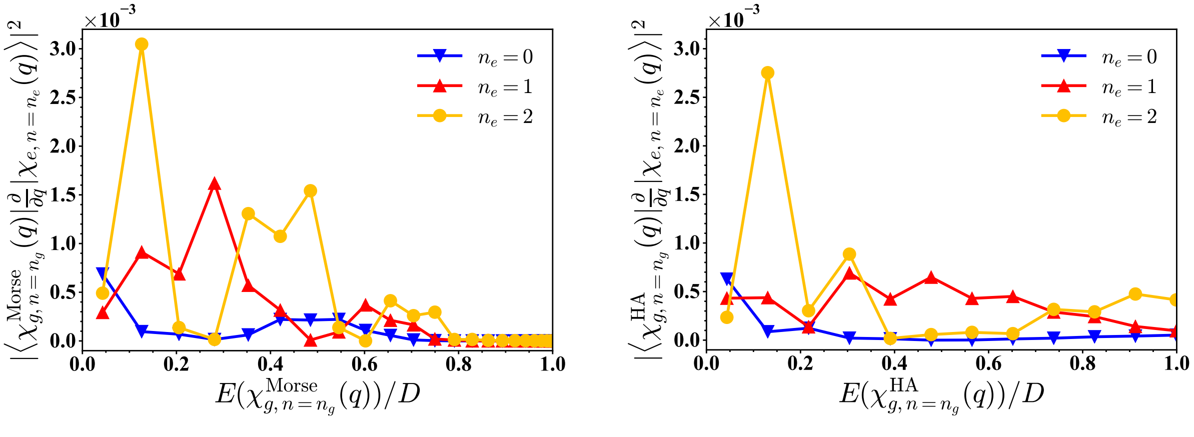

(a)

(b)

FIG. 7. The square of the matrix elements $\langle\chi_{\mathrm{e}}(q)|\frac{\partial}{\partial q}|\chi_{\mathrm{g}}(q)\rangle$ between different initial vibrational states of electronic excited state (distinguished by vibrational quanta n_{e}) and series of final vibrational states of electronic ground state (distinguished by the energy $E(\chi_{\mathrm{g},n})$) on a) Morse potential, b) harmonic potential under HA. Each triangle,inverted triangle or circle denotes a state with lines as a guide to the eye. The results are calculated through exact diagonalization. The displacement is $\Delta q = 0.7/\alpha$.

IV. CONCLUSION

In this work, we propose to use TD-DMRG to calculate the rate of molecular nonradiative electronic relaxation process based on the Fermi's golden rule. Firstly, we calculate the internal conversion rate of azulene under the harmonic approximation, in which the Duschinsky rotation effect is fully taken into consideration. The results are consistent with the analytically exact results calculated by the thermal vibration correlation function method and the computational scaling is polynomial, which demonstrates the effectiveness and scalability of the current method to be applied to large polyatomic molecules. Secondly, we calculate the internal conversion rate of a two-mode model system with Morse potential and assess the validity of harmonic approximation. We emphasize that the off-diagonal terms neglected in the former studies are also important to the transition rate and the harmonic approximation is unsatisfactory in a large parameter regime unless only the lowest several vibrational states of the lower electronic state are involved in the transition process when the adiabatic excitation energy is relatively low. Since the Morse potential is asymmetrical, the error of the harmonic approximation strongly depends on the direction of the shift of the excited state potential energy surface with respect to the ground state. When $\alpha\Delta q > 0$, the harmonic approximation will first underestimate the IC rate and then overestimate it as the excitation energy increases. This is due to that the amplitude of the wavefunction on the Morse potential is larger than that of the harmonic potential in the dissociative side but the wavefunction spreads quickly with energy while the harmonic wavefunction is much more localized. Hence, the Franck-Condon factor between the initial and final states on the Morse potential is first larger and then smaller than that under harmonic approximation. When $\alpha\Delta q < 0$, the harmonic approximation will slightly overestimate the IC rate because the wavefunction on the Morse potential is also localized on this side but the amplitude is smaller. Moreover, higher temperature will enlarge the error of harmonic approximation. It should be mentioned that though we focus on the rate of internal conversion process in the numerical examples in this work, the same approach could also be used in the calculation of the intersystem crossing rates. Finally, the potential energy surface of the real molecules is much more complicated than the simple Morse potential and thus the two-mode model is too ideal to fully describe the anharmonic effect on the rate of nonradiative electronic relaxation of real molecules. Therefore, applying the current TD-DMRG method to the real molecules with ab-initio anharmonic potential energy surface is worth further study.

SUPPLEMENTARY MATERIAL

See the supplementary material for the internal conversion rates k_{ic} calculated by TD-DMRG with different virtual bond dimension M_S and physical bond dimension d. Additional results with different Morse potential parameters can also be found.

ACKNOWLEDGMENTS

This work is supported by the National Natural Science Foundation of China (NSFC) through the project "Science CEnter for Luminescence from Molecular Aggregates (SCELMA)" Grant Number 21788102, as well as by the Ministry of Science and Technology of China through the National Key R&D Plan Grant Number 2017YFA0204501. J.R. is also supported by the NSFC via Grant Number 22003029.

REFERENCES

[1] N. J. Turro, *Modern molecular photochemistry* (University science books, 1991).

[2] R. Englman and J. Jortner, "The energy gap law for radiationless transitions in large molecules," Mol. Phys. **18**, 145–164 (1970).

[3] S. Lin, C. Chang, K. Liang, R. Chang, J. Zhang, T. Yang, M. Hayashi, Y. Shiu, and F. Hsu, "Ultrafast dynamics and spectroscopy of bacterial photosynthetic reaction centers," Adv. Chem. Phys. **121**, 1–88 (2002).

[4] Q. Shi and E. Geva, "Nonradiative electronic relaxation rate constants from approximations based on linearizing the path-integral forward- backward action," J. Phys. Chem. A **108**, 6109–6116 (2004).

[5] Q. Peng, Y. Yi, Z. Shuai, and J. Shao, "Excited state radiationless decay process with duschinsky rotation effect: formalism and implementation," J. Chem. Phys. **126**, 114302 (2007).

[6] R. Ianconescu, J. Tatchen, and E. Pollak, "On-the-fly semiclassical study of internal conversion rates of formaldehyde," J. Chem. Phys. **139**, 154311 (2013).

[7] S. Banerjee, A. Baiardi, J. Bloino, and V. Barone, "Temperature dependence of radiative and nonradiative rates from time-dependent correlation function methods," J. Chem. Theory Comput. **12**, 774–786 (2016).

[8] X. Sun and E. Geva, "Equilibrium fermi's golden rule charge transfer rate constants in the condensed phase: The linearized semiclassical method vs classical marcus theory," J. Phys. Chem. A **120**, 2976–2990 (2016).

[9] A. Celestino and A. Eisfeld, "Tuning nonradiative lifetimes via molecular aggregation," J. Phys. Chem. A **121**, 5948–5953 (2017).

[10] H.-D. Meyer, “Studying molecular quantum dynamics with the multiconfiguration time-dependent hartree method,” Wiley Interdiscip Rev Comput Mol Sci **2**, 351–374 (2012).

[11] G. Richings, I. Polyak, K. Spinlove, G. Worth, I. Burghardt, and B. Lasorne, “Quantum dynamics simulations using gaussian wavepackets: the vmcg method,” Int. Rev. Phys. Chem. **34**, 269–308 (2015).

[12] B. F. Curchod and T. J. Martínez, “Ab initio nonadiabatic quantum molecular dynamics,” Chem. Rev. **118**, 3305–3336 (2018).

[13] G. Cui and W. Thiel, “Generalized trajectory surface-hopping method for internal conversion and intersystem crossing,” J. Chem. Phys. **141**, 124101 (2014).

[14] R. Crespo-Otero and M. Barbatti, “Recent advances and perspectives on nonadiabatic mixed quantum-classical dynamics,” Chem. Rev. **118**, 7026–7068 (2018).

[15] L. Wang, J. Qiu, X. Bai, and J. Xu, “Surface hopping methods for nonadiabatic dynamics in extended systems,” Wiley Interdiscip Rev Comput Mol Sci **10**, e1435 (2020).

[16] M. H. Beck, A. Jäckle, G. A. Worth, and H.-D. Meyer, “The multiconfiguration time-dependent hartree (mctdh) method: a highly efficient algorithm for propagating wavepackets,” Phys. Rep. **324**, 1–105 (2000).

[17] S. N. Chowdhury and P. Huo, “Coherent state mapping ring polymer molecular dynamics for non-adiabatic quantum propagations,” J. Chem. Phys. **147**, 214109 (2017).

[18] X. Gao, Y. Lai, and E. Geva, “Simulating absorption spectra of multiexcitonic systems via quasiclassical mapping hamiltonian methods,” J. Chem. Theory Comput. **16**, 6465–6480 (2020).

[19] X. Gao and E. Geva, “A nonperturbative methodology for simulating multidimensional spectra of multiexcitonic molecular systems via quasiclassical mapping hamiltonian methods,” J. Chem. Theory Comput. **16**, 6491–6502 (2020).

[20] J. Zheng, J. Peng, Y. Xie, Y. Long, X. Ning, and Z. Lan, “Study of the exciton dynamics in perylene bisimide (pbi) aggregates with symmetrical quasiclassical dynamics based on the meyer–miller mapping hamiltonian,” Phys. Chem. Chem. Phys. **22**, 18192–18204 (2020).

[21] A. Toniolo, S. Olsen, L. Manohar, and T. J. Martinez, “Conical intersection dynamics in solution: the chromophore of green fluorescent protein,” Faraday Discuss. **127**, 149–63 (2004).

[22] Y. Liu, C. Li, Z. Ren, S. Yan, and M. R. Bryce, “All-organic thermally activated delayed fluorescence materials for organic light-emitting diodes,” Nat. Rev. Mater. **3**, 1–20 (2018).

[23] G. W. Robinson and R. P. Frosch, “Theory of electronic energy relaxation in the solid phase,” J. Chem. Phys. **37**, 1962–1973 (1962).

[24] G. W. Robinson and R. P. Frosch, "Electronic excitation transfer and relaxation," J. Chem. Phys. **38**, 1187–1203 (1963).

[25] S. H. Lin, "Rate of interconversion of electronic and vibrational energy," J. Chem. Phys. **44**, 3759–3767 (1966).

[26] S. H. Lin and R. Bersohn, "Effect of partial deuteration and temperature on triplet-state lifetimes," J. Chem. Phys. **48**, 2732–2736 (1968).

[27] Y. Niu, Q. Peng, and Z. Shuai, "Promoting-mode free formalism for excited state radiationless decay process with duschinsky rotation effect," Science in China Series B: Chemistry **51**, 1153–1158 (2008).

[28] Y. Niu, Q. Peng, C. Deng, X. Gao, and Z. Shuai, "Theory of excited state decays and optical spectra: application to polyatomic molecules," J. Phys. Chem. A **114**, 7817–7831 (2010).

[29] Q. Peng, Y. Niu, Q. Shi, X. Gao, and Z. Shuai, "Correlation function formalism for triplet excited state decay: Combined spin-orbit and nonadiabatic couplings," J. Chem. Theory Comput. **9**, 1132–43 (2013).

[30] Q. Peng, Y. Yi, Z. Shuai, and J. Shao, "Toward quantitative prediction of molecular fluorescence quantum efficiency: role of duschinsky rotation," J. Am. Chem. Soc. **129**, 9333–9 (2007).

[31] R. Ianconescu and E. Pollak, "Semiclassical initial value representation study of internal conversion rates," J. Chem. Phys. **134**, 234305 (2011).

[32] A. Humeniuk, M. Buzancic, J. Hoche, J. Cerezo, R. Mitric, F. Santoro, and V. Bonacic-Koutecky, "Predicting fluorescence quantum yields for molecules in solution: A critical assessment of the harmonic approximation and the choice of the lineshape function," J. Chem. Phys. **152**, 054107 (2020).

[33] S. R. White, "Density matrix formulation for quantum renormalization groups," Phys. Rev. Lett. **69**, 2863–2866 (1992).

[34] S. R. White, "Density-matrix algorithms for quantum renormalization groups," Phys. Rev. B **48**, 10345–10356 (1993).

[35] G. Vidal, "Efficient simulation of one-dimensional quantum many-body systems," Phys. Rev. Lett. **93**, 040502 (2004).

[36] S. R. White and A. E. Feiguin, "Real-time evolution using the density matrix renormalization group," Phys. Rev. Lett. **93**, 076401 (2004).

[37] A. W. Chin, J. Prior, R. Rosenbach, F. Caycedo-Soler, S. F. Huelga, and M. B. Plenio, "The role of non-equilibrium vibrational structures in electronic coherence and recoherence in pig-

ment–protein complexes," Nat. Phys. **9**, 113–118 (2013).

[38] E. Ronca, Z. Li, C. A. Jimenez-Hoyos, and G. K.-L. Chan, "Time-step targeting time-dependent and dynamical density matrix renormalization group algorithms with ab initio hamiltonians," J. Chem. Theory Comput. **13**, 5560–5571 (2017).

[39] Y. Yao, K.-W. Sun, Z. Luo, and H. Ma, "Full quantum dynamics simulation of a realistic molecular system using the adaptive time-dependent density matrix renormalization group method," J. Phys. Chem. Lett. **9**, 413–419 (2018).

[40] J. Ren, Z. Shuai, and G. Kin-Lic Chan, "Time-dependent density matrix renormalization group algorithms for nearly exact absorption and fluorescence spectra of molecular aggregates at both zero and finite temperature," J. Chem. Theory Comput. **14**, 5027–5039 (2018).

[41] A. Baiardi and M. Reiher, "Large-scale quantum dynamics with matrix product states," J. Chem. Theory Comput. **15**, 3481–3498 (2019).

[42] B. Kloss, D. R. Reichman, and R. Tempelaar, "Multiset matrix product state calculations reveal mobile franck-condon excitations under strong holstein-type coupling," Phys. Rev. Lett. **123**, 126601 (2019).

[43] X. Xie, Y. Liu, Y. Yao, U. Schollwock, C. Liu, and H. Ma, "Time-dependent density matrix renormalization group quantum dynamics for realistic chemical systems," J. Chem. Phys. **151**, 224101 (2019).

[44] W. Li, J. Ren, and Z. Shuai, "Finite-temperature td-dmrg for the carrier mobility of organic semiconductors," J. Phys. Chem. Lett. **11**, 4930–4936 (2020).

[45] C. Hubig, I. McCulloch, and U. Schollwöck, "Generic construction of efficient matrix product operators," Phys. Rev. B **95**, 035129 (2017).

[46] J. Ren, W. Li, T. Jiang, and Z. Shuai, "A general automatic method for optimal construction of matrix product operators using bipartite graph theory," J. Chem. Phys. **153**, 084118 (2020).

[47] A. Jäckle and H.-D. Meyer, "Product representation of potential energy surfaces," J. Chem. Phys. **104**, 7974–7984 (1996).

[48] S. Manzhos and T. Carrington Jr, "Using neural networks to represent potential surfaces as sums of products," J. Chem. Phys. **125**, 194105 (2006).

[49] A. E. Feiguin and S. R. White, "Finite-temperature density matrix renormalization using an enlarged hilbert space," Phys. Rev. B **72**, 220401 (2005).

[50] U. Schollwöck, "The density-matrix renormalization group in the age of matrix product states," Ann. Phys. **326**, 96–192 (2011).

[51]G. Li, C. Rosenthal, and H. Rabitz, "High dimensional model representations," J. Phys. Chem. A **105**, 7765–7777 (2001).

[52]J. M. Bowman, S. Carter, and X. Huang, "Multimode: a code to calculate rovibrational energies of polyatomic molecules," Int. Rev. Phys. Chem. **22**, 533–549 (2003).

[53]V. Barone, M. Biczysko, J. Bloino, M. Borkowska-Panek, I. Carnimeo, and P. Panek, "Toward anharmonic computations of vibrational spectra for large molecular systems," Int. J. Quantum Chem. **112**, 2185–2200 (2012).

[54]M. Sibaev and D. Crittenden, "An efficient and numerically stable procedure for generating sextic force fields in normal mode coordinates," J. Chem. Phys. **144**, 214107 (2016).

[55]J. R. Reimers, "A practical method for the use of curvilinear coordinates in calculations of normal-mode-projected displacements and duschinsky rotation matrices for large molecules," J. Chem. Phys. **115**, 9103–9109 (2001).

[56]A. Baiardi, J. Bloino, and V. Barone, "Accurate simulation of resonance-raman spectra of flexible molecules: An internal coordinates approach," J. Chem. Theory Comput. **11**, 3267–3280 (2015).

[57]J. Light, I. Hamilton, and J. Lill, "Generalized discrete variable approximation in quantum mechanics," J. Chem. Phys. **82**, 1400–1409 (1985).

[58]S. Paeckel, T. Köhler, A. Swoboda, S. R. Manmana, U. Schollwöck, and C. Hubig, "Time-evolution methods for matrix-product states," Ann. Phys. **411**, 167998 (2019).

[59]W. Li, J. Ren, and Z. Shuai, "Numerical assessment for accuracy and gpu acceleration of td-dmrg time evolution schemes," J. Chem. Phys. **152**, 024127 (2020).

[60]H.-D. Meyer and H. Wang, "On regularizing the mctdh equations of motion," J. Chem. Phys. **148**, 124105 (2018).

[61]"Renormalizer," `https://github.com/shuaigroup/Renormalizer`.

[62]Z. Shuai, "Thermal vibration correlation function formalism for molecular excited state decay rates," Chin. J. Chem **38**, 1223–1232 (2020).

[63]M. J. Frisch, G. W. Trucks, H. B. Schlegel, G. E. Scuseria, M. A. Robb, J. R. Cheeseman, G. Scalmani, V. Barone, G. A. Petersson, H. Nakatsuji, X. Li, M. Caricato, A. V. Marenich, J. Bloino, B. G. Janesko, R. Gomperts, B. Mennucci, H. P. Hratchian, J. V. Ortiz, A. F. Izmaylov, J. L. Sonnenberg, D. Williams-Young, F. Ding, F. Lipparini, F. Egidi, J. Goings, B. Peng, A. Petrone, T. Henderson, D. Ranasinghe, V. G. Zakrzewski, J. Gao, N. Rega, G. Zheng, W. Liang, M. Hada, M. Ehara, K. Toyota, R. Fukuda, J. Hasegawa, M. Ishida, T. Nakajima,

Y. Honda, O. Kitao, H. Nakai, T. Vreven, K. Throssell, J. A. Montgomery, Jr., J. E. Peralta, F. Ogliaro, M. J. Bearpark, J. J. Heyd, E. N. Brothers, K. N. Kudin, V. N. Staroverov, T. A. Keith, R. Kobayashi, J. Normand, K. Raghavachari, A. P. Rendell, J. C. Burant, S. S. Iyengar, J. Tomasi, M. Cossi, J. M. Millam, M. Klene, C. Adamo, R. Cammi, J. W. Ochterski, R. L. Martin, K. Morokuma, O. Farkas, J. B. Foresman, and D. J. Fox, "Gaussian~16 Revision C.01," (2016), gaussian Inc. Wallingford CT.

[64] X.-K. Chen, Y. Tsuchiya, Y. Ishikawa, C. Zhong, C. Adachi, and J.-L. Brédas, "A new design strategy for efficient thermally activated delayed fluorescence organic emitters: from twisted to planar structures," Adv. Mater. **29**, 1702767 (2017).

DATA AVAILABILITY

The data that support the findings of this study are available from the corresponding author upon reasonable request.

Supplementary materials for "Evaluating the anharmonicity contributions to the molecular excited state internal conversion rates with finite temperature TD-DMRG"

Yuanheng Wang, Jiajun Ren,[*] and Zhigang Shuai[†]
MOE Key Laboratory of Organic OptoElectronics and Molecular Engineering,
Department of Chemistry, Tsinghua University, Beijing 100084, People's Republic of China

(Dated: April 1, 2021)

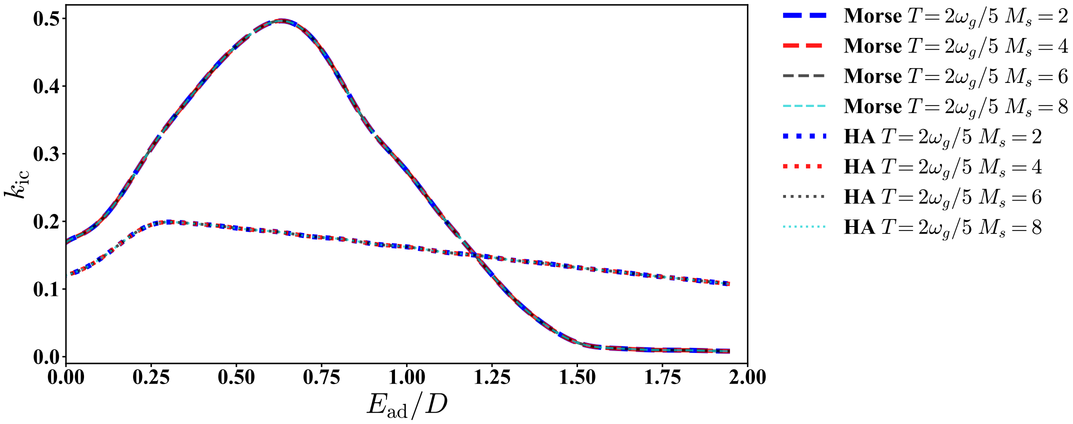

FIG. 1. The convergence of the bond dimensions M_S for MPS in the two-mode model used in the main text. The displacement $\Delta q = 0.7/\alpha$. the temperature $T = 2\omega_g/5$, the physical bond dimension $d = 100$ .The result indicates that $M_S = 4$ is large enough in this calculation.

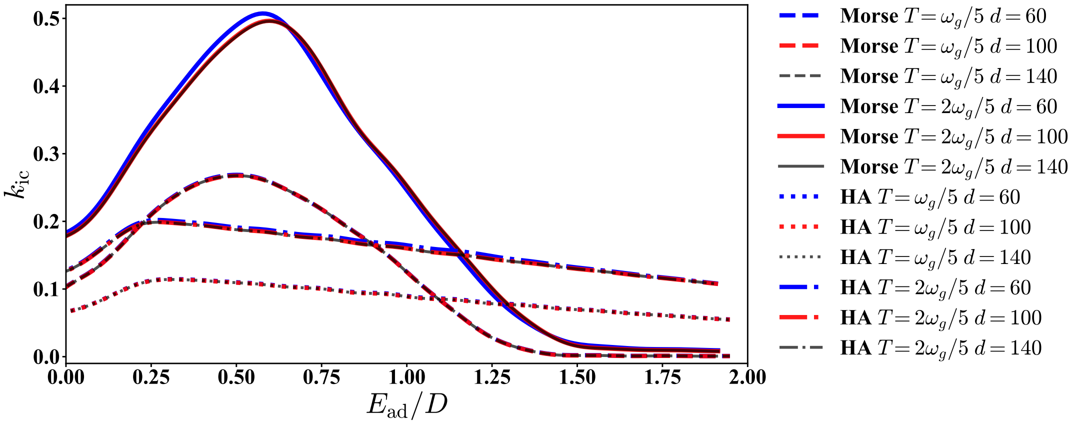

FIG. 2. The convergence of the primitive basis set (simple harmonic oscillator basis) in the two-mode model used in the main text. The displacement $\Delta q = 0.7/\alpha$. With all the temperatures considered, the results with physical bond dimension $d = 100$ and $d = 140$ are the same, indicating that $d = 100$ is large enough in this calculation.

---

[*] renjj@mail.tsinghua.edu.cn
[†] zgshuai@tsinghua.edu.cn

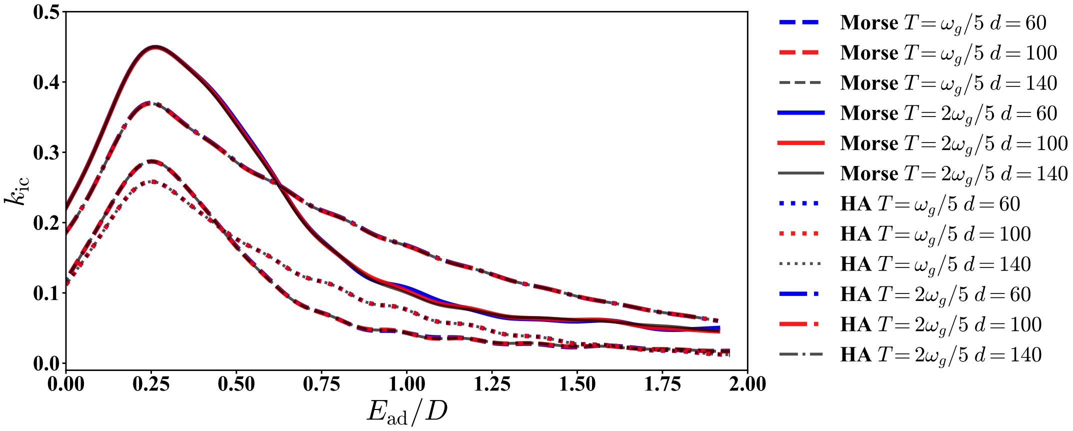

FIG. 3. The convergence of the primitive basis set (simple harmonic oscillator basis) in the two-mode model used in the main text. The displacement $\Delta q = 0/\alpha$. With all the temperatures considered, the results with physical bond dimension $d = 100$ and $d = 140$ are the same, indicating that $d = 100$ is large enough in this calculation.

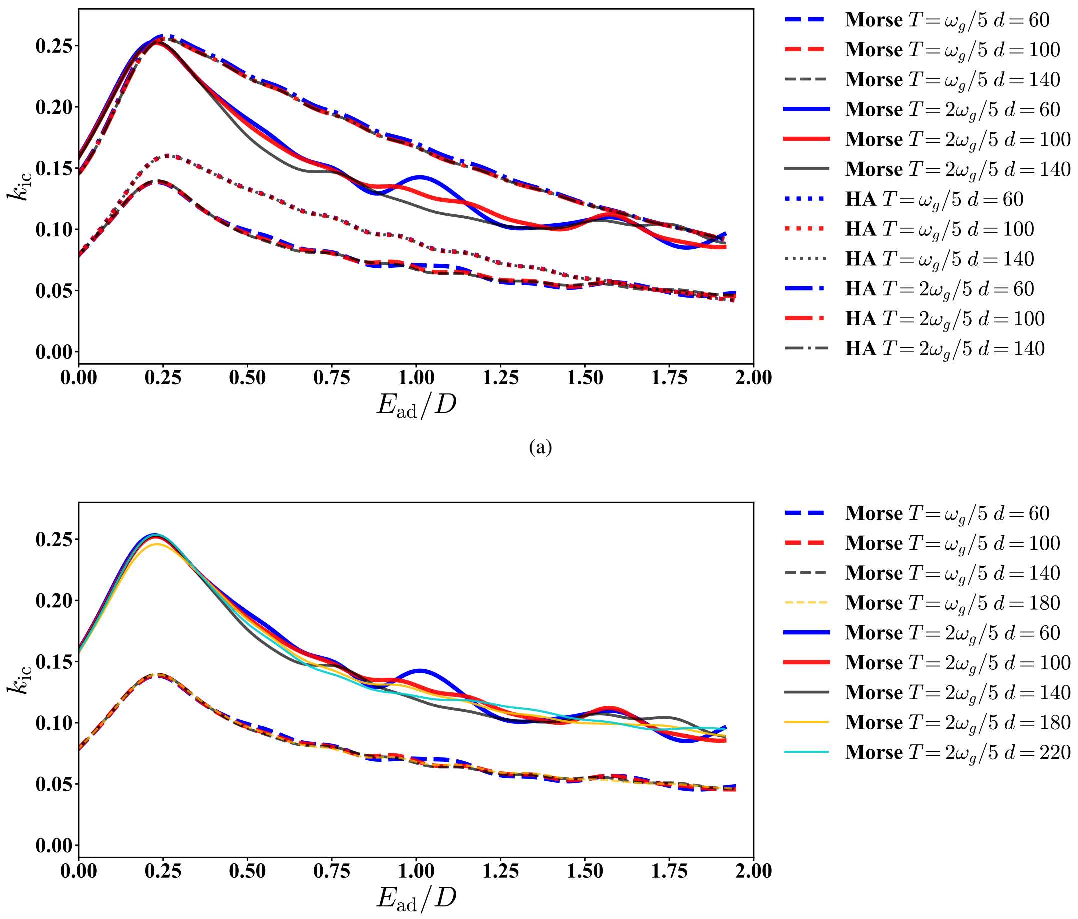

(a)

(b)

FIG. 4. (a). The convergence of the primitive basis set (simple harmonic oscillator basis) in the two-mode model used in the main text. The displacement $\Delta q = -0.52/\alpha$. The results with $d = 100$ are consistent with that of $d = 140$ except the Morse potential with $T = 2\omega_g/5$. (b). For Morse potential with $T = 2\omega_g/5$, larger basis set is tested. With d up to 220, k_{ic} is still not converged in the high energy region. However, considering the error caused by the insufficient basis in this case dose not change the relative relationship between the internal conversion rate calculated from Morse potential and its harmonic approximation, we still use $d = 100$ in the main text for higher efficiency.

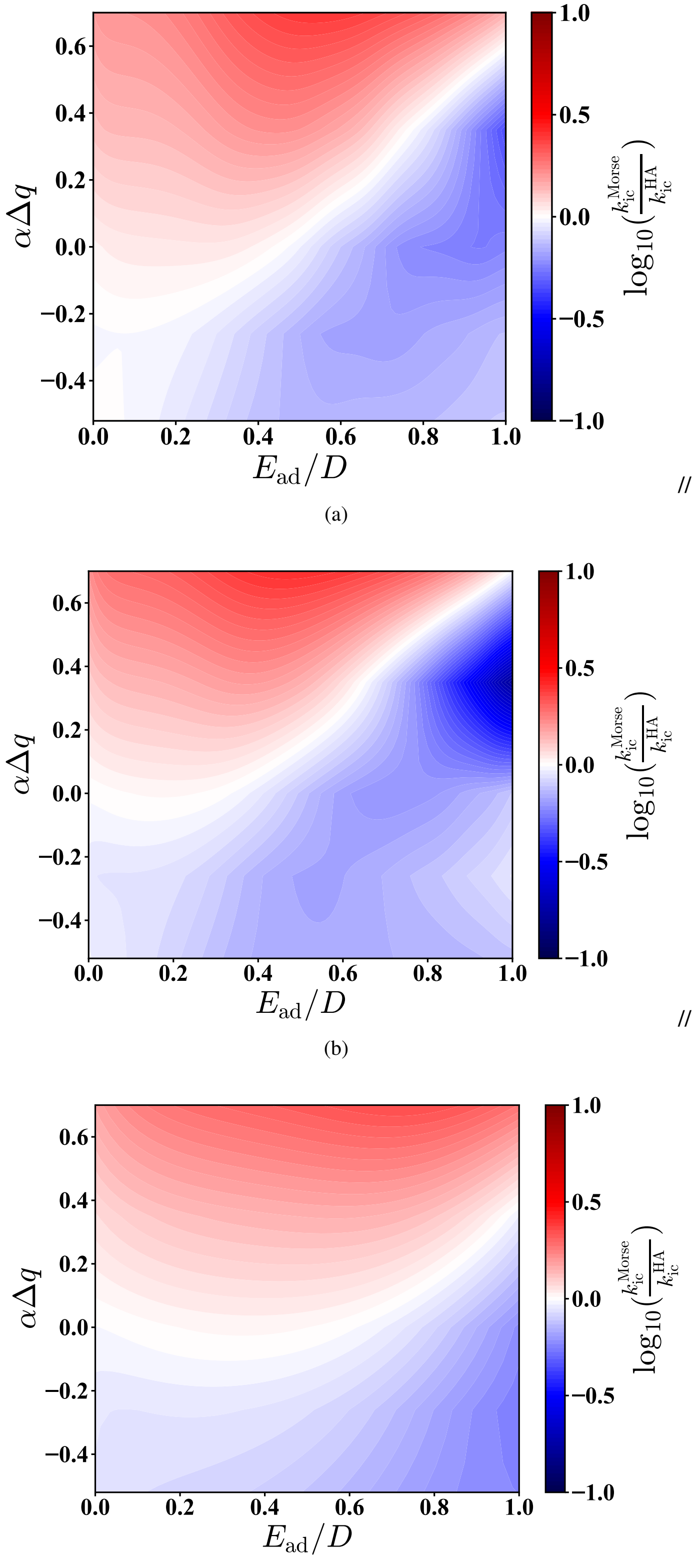

(a)

(b)

(c)

FIG. 5. (a), (b) and (c) show the ratio of the internal conversion rate on the Morse potential with respect to that under HA with different displacements and adiabatic excitation energies. (a). $D = D_0$, $\alpha = \alpha_0$. The same as Fig. 5a in the main text. (b). $D = D_0$, $\alpha = 2/3\alpha_0$. (c). $D = 4/9D_0$, $\alpha = \alpha_0$. In all cases, $D_0 = 5.52\,\mathrm{eV}$, $\alpha_0 = 2.23\,\mathrm{amu}^{-1/2}\text{Å}^{-1}$, $\omega_e = \omega_g/5$ and $T = \omega_g/5$. The parameter for TD-DMRG calculations are all $d = 100$, $M_s = 4$.